Addendum: B-Spline Interpolation in Medical Image Processing

Thomas M. Lehmann , *Member, IEEE*, Claudia Gönner, and Klaus Spitzer

***Abstract*—This paper analyzes B-spline interpolation techniques of degree 2, 4, and 5 with respect to all criteria that have been applied to evaluate various interpolation schemes in a recently published survey on image interpolation in medical imaging (Lehmann *et al.*, 1999). It is shown that high-degree B-spline interpolation has superior Fourier properties, smallest interpolation error, and reasonable computing times. Therefore, high-degree B-splines are preferable interpolators for numerous applications in medical image processing, particularly if high precision is required. If no aliasing occurs, this result neither depends on the geometric transform applied for the tests nor the actual content of images.**

***Index Terms*—Aliasing, B-splines, image resampling, interpolation.**

I. Introduction

Image interpolation is frequently applied in medical imaging and novel techniques are continuously being introduced. Therefore, a comprehensive survey of existing interpolation methods has recently been published [1]. A uniform notation for all methods was introduced and basic criteria, such as interpolation versus approximation as well as dc-constancy versus dc-inconstancy have been defined. Furthermore, it was shown that the ideal interpolator has a rectangular shape in the frequency domain, which corresponds to an infinite impulse response in the spatial domain (Fig. 1). Ideal interpolation, windowed and truncated sinc interpolation, linear, quadratic, and cubic approximation and interpolation schemes, B-spline interpolation of degree 3, as well as Lagrange and Gaussian methods of different orders and kernel sizes were reviewed in detail. In particluar, these methods were compared with respect to spatial and Fourier analyses, computational complexity as well as runtime evaluations, and qualitative and quantitative interpolation error determinations for particular interpolation tasks, which were taken from common situations in medical image processing. In this addendum, the survey is extended to B-spline interpolation of degree 2, 4, and 5.

Manuscript received September 18, 2000; revised April 12, 2001. The Associate Editor responsible for coordinating the review of this paper and recommending its publication was M. W. Vannier. *Asterisk indicates corresponding author.*

*T. M. Lehmann is with the Institute of Medical Informatics, Aachen University of Technology (RWTH), Pauwelsstrasse 30, D-52057 Aachen, Germany (e-mail: lehmann@computer.org).

C. Gönner and K. Spitzer are with the Institute of Medical Informatics, Aachen University of Technology (RWTH), D-52057 Aachen, Germany.

Publisher Item Identifier S 0278-0062(01)05363-0.

II. B-Spline Interpolation

Using the notation of [1], the order N determines the number of supporting points of kernels with finite impulse response (FIR). Basis spline (B-spline) approximators of order $N, h_N(x)$, are piecewise polynomials of degree $M = N - 1$. They are obtained from the M-fold self-convolution of the rectangular pulse $h_1(x)$ that determines the nearest neighbor interpolation kernel [1, Eq. (11)]. Therefore, the frequency response $H_N(f)$ of FIR-spline approximators with N supporting points yields

$$H_N(f) = \mathrm{sinc}(f)^N \tag{1}$$

with

$$\mathrm{sinc}(x) = \frac{\sin(\pi x)}{\pi x}.$$

The approximator kernel's explicit formula is given by [2]

$$h_N(x) = \frac{1}{(N-1)!}\sum_{n=0}^{N}\binom{N}{n}(-1)^n\left(x - n + \frac{N}{2}\right)_+^{N-1} \tag{2}$$

where $(x)_+^y$ denotes the one-sided power function

$$(x)_+^y = \begin{cases} x^y, & x \geq 0 \\ 0, & x < 0 \end{cases}.$$

The polynomial spline interpolant with infinite support has the form of [1, Eq. (15)]

$$s_M(x) = \sum_k t(k) \cdot h_N(x - k) \tag{3}$$

where the $t(k)$ are derived from the image's sample points $s(k)$ in such a way that the resulting curve interpolates the discrete image. For B-spline interpolation of degree $M = 2$, 4, and 5 ([1, Eq. (16)] for the cubic case of $M = 3$) we obtain [3]

$$\begin{aligned} s_2(k) &= \frac{1}{8}(t(k-1) + 6t(k) + t(k+1)) \\ s_4(k) &= \frac{1}{384}(t(k-2) + 76t(k-1) + 230t(k) \\ &\quad + 76t(k+1) + t(k+2)) \\ s_5(k) &= \frac{1}{120}(t(k-2) + 26t(k-1) + 66t(k) \\ &\quad + 26t(k+1) + t(k+2)). \end{aligned} \tag{4}$$

Similar to the cubic B-spline, which is derived in detail in [1], the B-spline coefficients $t(k)$ are obtained from the solution of a linear system of equations that involves a band diag-

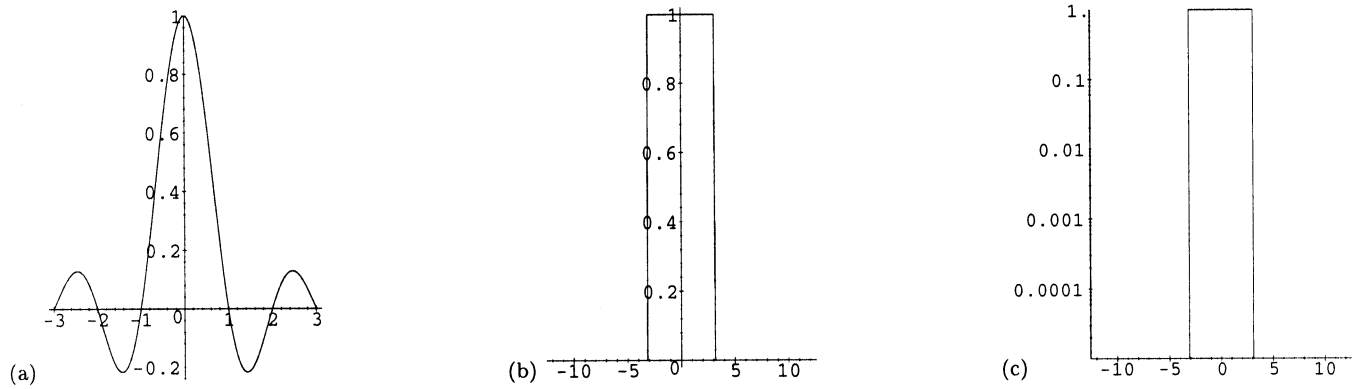

Fig. 1. Ideal interpolation. (a) Kernel plotted for $|x| < 3$. (b) Magnitude of Fourier transform. (c) Logarithmic plot of magnitude.

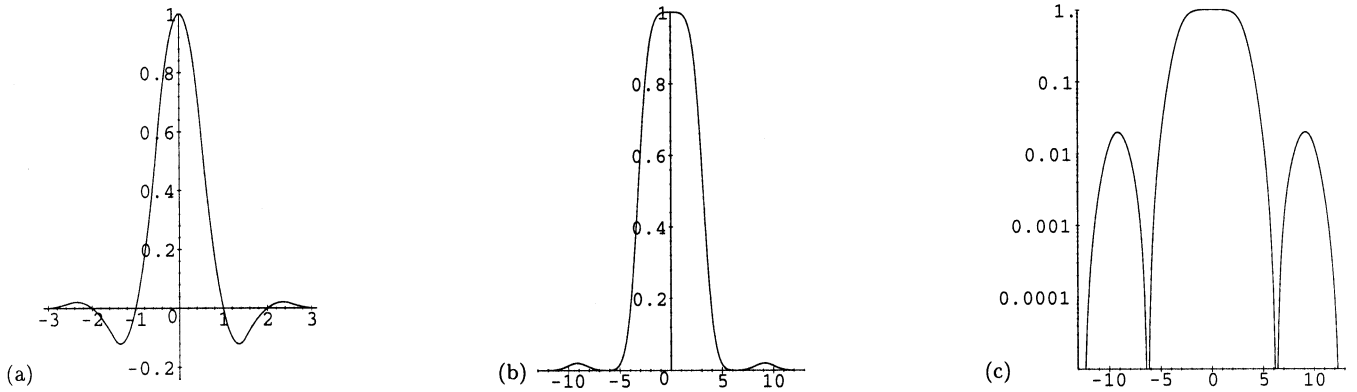

Fig. 2. B-spline interpolation of degree $M = 2$. (a) Kernel plotted for $|x| < 3$. (b) Magnitude of Fourier transform. (c) Logarithmic plot of magnitude.

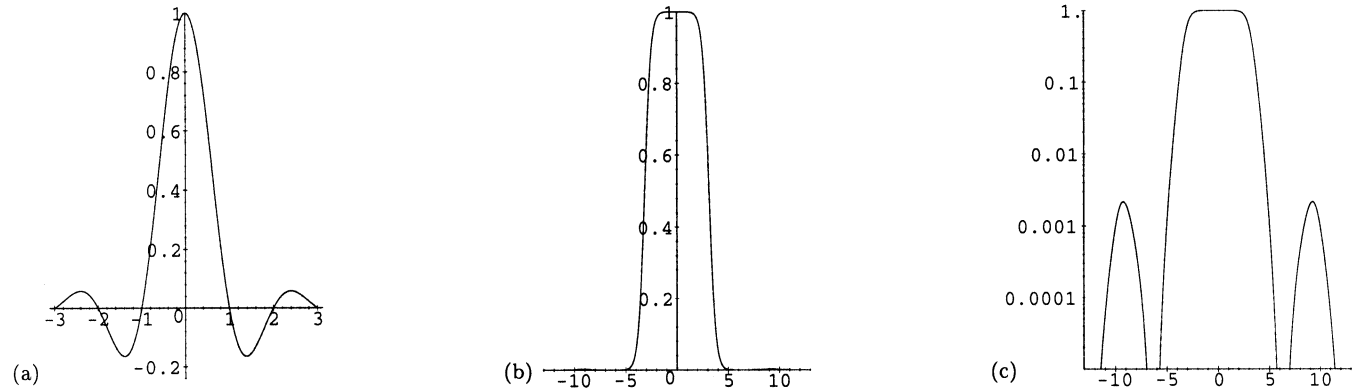

Fig. 3. B-spline interpolation of degree $M = 4$. (a) Kernel plotted for $|x| < 3$. (b) Magnitude of Fourier transform. (c) Logarithmic plot of magnitude.

onal Toeplitz matrix [4]. The solution can be obtained most efficiently by recursive digital filtering as described in [3] and [4]. By performing the same type of manipulation as in the cubic case, we can apply the digital filter to the B-spline basis functions and obtain an explicit expression for both the frequency response of the spline interpolator [5], [6]

$$ {}^{\text{Spline}}H_M(f) = \frac{[\text{sinc}(f)]^{(M+1)}}{\sum_{k=-\infty}^{\infty}[\text{sinc}(f-k)]^{(M+1)}} \qquad (5) $$

as well as its infinite impulse response (IIR) ([1, Eq. (21)] for $M = 3$)

$$ {}^{\text{Spline}}h_2(x) = \sqrt{2}\sum_{k=-\infty}^{\infty}(\sqrt{8}-3)^{|k|}\cdot h_3(x+k) $$

$$ {}^{\text{Spline}}h_4(x) = \sum_{k=-\infty}^{\infty}\Big(2.288\,319\cdot(-0.361\,34)^{|k|} - 0.075\,586\cdot(-0.013\,73)^{|k|}\Big)\cdot h_5(x+k) $$

$$ {}^{\text{Spline}}h_5(x) = \sum_{k=-\infty}^{\infty}\Big(3.094\,986\cdot(-0.430\,575)^{|k|} - 0.252\,816\cdot(-0.043\,096)^{|k|}\Big)\cdot h_6(x+k). \qquad (6) $$

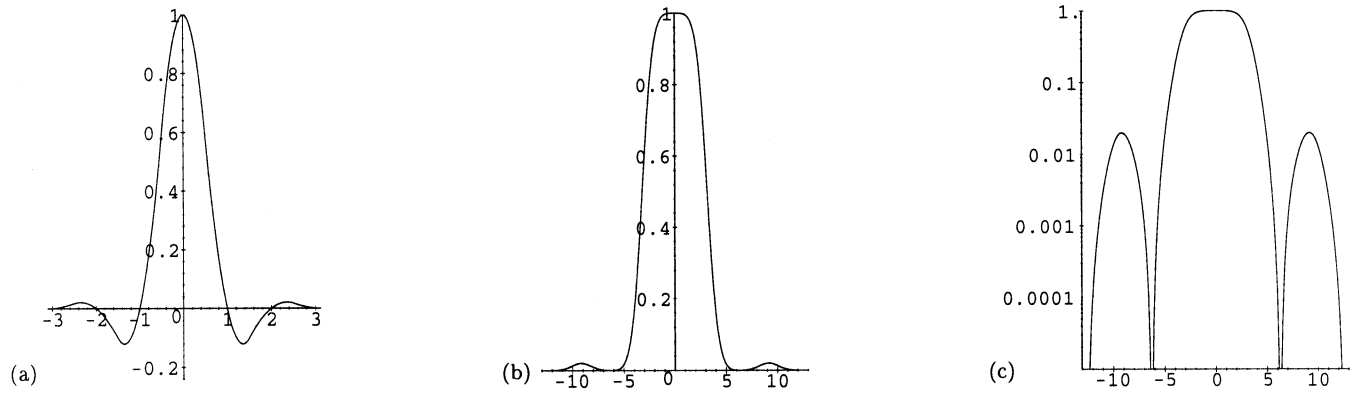

Fig. 4. B-spline interpolation of degree $M = 5$. (a) Kernel plotted for $|x| < 3$. (b) Magnitude of Fourier transform. (c) Logarithmic plot of magnitude.

The B-spline approximators $h_N(x)$ are indicated by the number N of supporting points. Since B-spline interpolators ${}^{\mathrm{Spline}}h_M(x)$ have infinite supporting points, they are indexed by the degree M of polynomial splines. However, all IIR-filters ${}^{\mathrm{Spline}}h_M(x)$ have exponential decay [2]. The plots corresponding to the spline interpolators of degree 2, 4, and 5 are given in Figs. 2–4, respectively, while that of degree 3 is plotted in [1, Fig. 14]. Note that B-spline interpolators of higher degree tend to be more and more sinc-like while their frequency responses get closer to the ideal lowpass filter. In fact, it has been proven that the B-spline interpolators convergence to the ideal bandlimited one as the degree tends to infinity [5], [6]. An additional important property of B-spline interpolators is that they perfectly reproduce all polynomials up to the degree M. In particular, this implies that they all satisfy the partition of unity condition, which is equivalent to their dc-constancy [1].

III. Results

The IIR kernels were compared in various situations typically encountered in medical applications. As it was done in the survey [1], the efficiency and accuracy were evaluated by analyzing Fourier properties, visual quality, interpolation error, complexity, and runtime.

A. Fourier Analysis

The frequency analysis of Figs. 2–4 was focused on three characteristics: passband $|\omega| < \pi$, cutoff point $|\omega| = \pi$, and stopband $|\omega| > \pi$. The passband characteristics of all B-spline interpolators were similar to that of the ideal interpolator (Fig. 5). The constant gain equaled one until closely approaching the cutoff point, especially for high degrees of B-splines ($M = 5$). Hence, only the highest frequency components were smoothed by B-spline interpolation. Increasing the degree M of B-spline interpolation improved the passband characteristic by enlargement of the flat ridge at $H_M(0)$. Furthermore, the absolute slope of the kernel's frequency response at the cutoff point was increased, also improving the frequency response of the interpolator for higher degrees of B-spline interpolation. In addition, the higher the degree of B-spline interpolation, the lower the sidelobes within the stopband. For $M = 5$, sidelobes were below 1%. In comparison to all other kernels [1, Figs. 5–24], B-spline interpolation of high degree ($M = 5$) had a frequency response closest to that of the ideal interpolator.

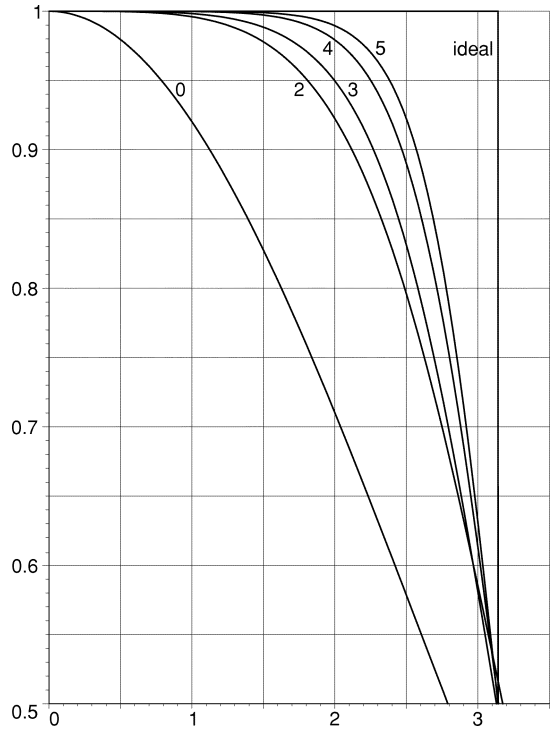

Fig. 5. Fourier transforms of B-spline interpolation of degrees $M = 0$, 2, 3, 4, 5, and ∞ within the passband $|\omega| < \pi$, zoomed from panel (b) of Figs. 1–4.

B. Interpolation Quality

A sharply focused 8-bit photograph of a human eye [Fig. 6(a)] was interpolated by each of the B-spline interpolation methods (as well as linear interpolation) to correct the photograph's aspect ratio. To visualize the interpolation error, the aspect-ratio-corrected image was interpolated again for downsizing to its initial dimension. The same interpolation method was used for both forward and backward transformation.

The interpolation quality was assessed visually by the pixelwise absolute difference of the original photograph with the transformed photograph. All pixels that differ more than one grey scale unit are shown in black, while all others are displayed in white. The subtractions in Fig. 6 appreciably demonstrate the superior quality of B-spline interpolation as compared to linear

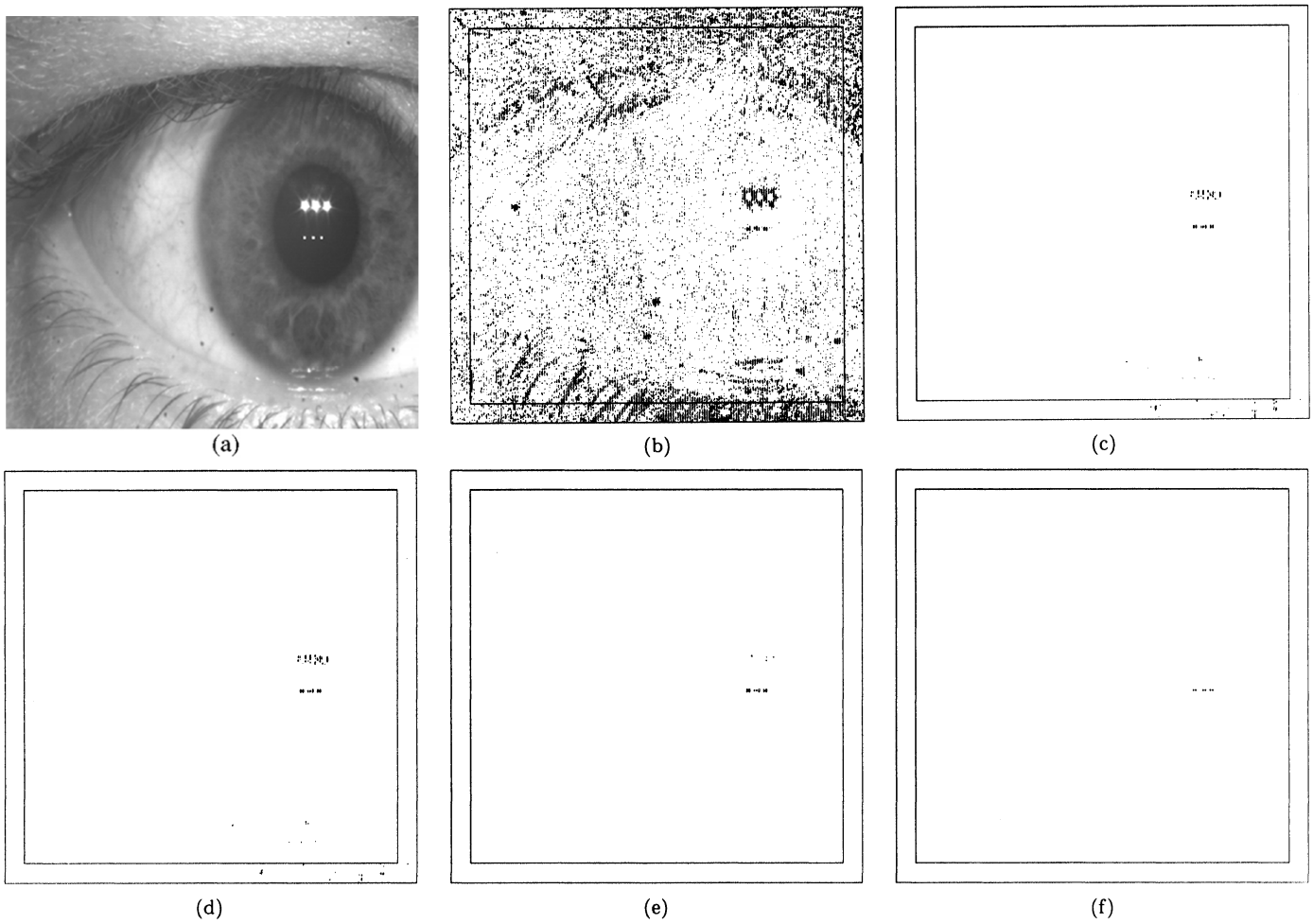

Fig. 6. Results of aspect ratio correction of a photograph (extends [1, Fig. 27]). Pixels with error >1.0 are displayed in black. The frame indicates the inner area for quantitative error comparisons ignoring border effects: (a) Original photograph (512 $\times$ 512, 8-bit). (b) Linear interpolation. (c)–(f) B-spline interpolation of degree $M = 2$ through $M = 5$, respectively.

interpolation. Note that all error images contain only very few black pixels, which are located at image regions of highest contrast. In particular, B-spline interpolation of degree 4 and 5 [Fig. 6(e) and (f), respectively] result in the lowest number of error pixels when compared to all other methods [1, Fig. 27].

C. Quantitative Error Analysis

All quantitative comparisons of the interpolation quality were based on the normalized cross-correlation coefficient, C [1, Eq. (34)], calculated within a centered subimage before and after distorting the image forward and backward. The subimage size of 462 $\times$ 462 out of 512 $\times$ 512 pixel is marked by the inner frame in Fig. 6(b)–(f). It was chosen to avoid border effects of kernels with large support. Those effects are a minor problem in medical image processing, because important details are usually centered. In addition, a linear score, S_C [1, Eq. (35)], was computed to rank-order all similarities by setting the linear method to zero and the cubic B-spline interpolation to one.

Table I shows the similarities C and scores S_C obtained by the aspect ratio correction of the eye image [Fig. 6(a)]. While the scores for the Lagrange kernels of sizes $N = 5$ and $N = 7$ were shown to exceed that for the cubic B-spline interpolator [1], the scores for the B-spline interpolators of degree 4 and 5 were larger compared with all other techniques [1, Table II].

A second interpolation evaluation was performed by rotating a 12-bit magnetic resonance image (MRI). In contrast to

TABLE I
RESULTS OF ASPECT RATIO CORRECTION OF THE PHOTOGRAPH (EXTENDS [1, TABLE II])

Interpolation sheme	N	Degree	C	S_C
Linear	2×2	—	0.9999217	0
B-spline (interpol.)	—	$M = 2$	0.9999974	0.99
B-spline (interpol.)	—	$M = 3$	0.9999979	1
B-spline (interpol.)	—	$M = 4$	0.9999996	1.02
B-spline (interpol.)	—	$M = 5$	0.9999998	1.02

TABLE II
RESULTS OF ROTATING THE MR IMAGE (EXTENDS [1, TABLE III])

Interpolation sheme	N	Degree	Mean(C)	StD(C)	S_C
Linear	2×2	—	0.9979303	$0.23633 \cdot 10^{-4}$	0
B-spline (interpol.)	—	$M = 2$	0.9998330	$0.08468 \cdot 10^{-4}$	0.98
B-spline (interpol.)	—	$M = 3$	0.9998789	$0.09218 \cdot 10^{-4}$	1
B-spline (interpol.)	—	$M = 4$	0.9999214	$0.05941 \cdot 10^{-4}$	1.02
B-spline (interpol.)	—	$M = 5$	0.9999342	$0.04559 \cdot 10^{-4}$	1.03

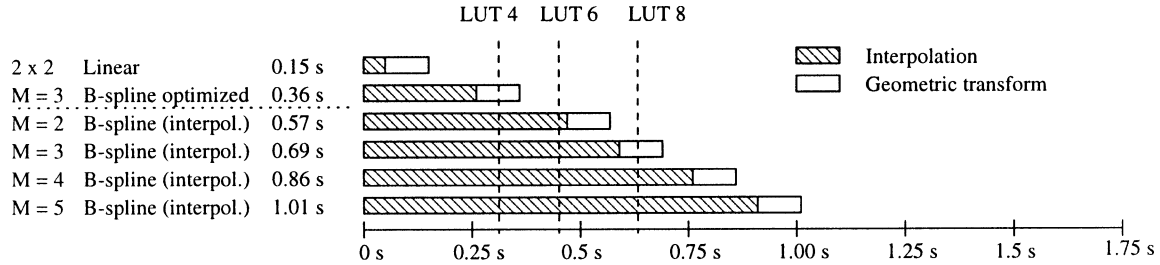

Fig. 7. Runtimes measured on a Sparc Ultra 1 (extends [1, Fig. 28]). The runtimes refer to the entire task: interpolation and geometric transform. Limits resulting from implementation via look-up tables (LUTs) of $N \times N$ FIR kernels filled with 10 000 elements per unit are given for $N = 4$, 6, and 8.

TABLE III
RESULTS OF PESPECTIVE PROJECTION OF X-RAY IMAGES (EXTENDS [1, TABLE IV])

Interpolation sheme	N	Degree	Mean(C)	StD(C)	S_C
Linear	2×2	—	0.9980701	$5.25685 \cdot 10^{-4}$	0
B-spline (interpol.)	—	$M = 2$	0.9987111	$3.81488 \cdot 10^{-4}$	1.01
B-spline (interpol.)	—	$M = 3$	0.9987056	$3.89628 \cdot 10^{-4}$	1
B-spline (interpol.)	—	$M = 4$	0.9986471	$4.12559 \cdot 10^{-4}$	0.91
B-spline (interpol.)	—	$M = 5$	0.9985933	$4.28824 \cdot 10^{-4}$	0.82

TABLE IV
RESULTS OF PESPECTIVE PROJECTION OF X-RAY IMAGES (NONALIASING)

Interpolation sheme	N	Degree	Mean(C)	StD(C)	S_C
Linear	2×2	—	0.9992947	$1.82241 \cdot 10^{-4}$	0
B-spline (interpol.)	—	$M = 2$	0.9998981	$0.34120 \cdot 10^{-4}$	0.99
B-spline (interpol.)	—	$M = 3$	0.9999072	$0.32507 \cdot 10^{-4}$	1
B-spline (interpol.)	—	$M = 4$	0.9999335	$0.24844 \cdot 10^{-4}$	1.04
B-spline (interpol.)	—	$M = 5$	0.9999403	$0.23026 \cdot 10^{-4}$	1.05

the goemetries in the prior case of aspect ratio correction, the number of pixels contributing to the image was nearly unchanged, and almost all 256×256 pixels had to be recalculated for both forward and backward rotation. The 50 normal distributed angles from [1] have been used for quantitative evaluation of interpolation errors. The mean correlation and standard deviation of corresponding forward and backward rotations, Mean(C) and StD(C), respectively, are summarized in Table II. They were scored in the same fashion as in the previous example. Again, higher degree B-spline interpolation was scored larger than 1.0 and, hence, outperformed all other techniques for this quantitative evaluation [1, Table III]. Note that the improvement obtained by stepwise increasing the degree of B-spline interpolation was statistically significant for each step (Student's t-test, $p \ll 0.005$).

In a third evaluation, a set of 50 radiographs were chosen arbitrarily from clinical records [1]. They were projected perspectively both forward and backward. Again, the standard deviation of the interpolation error as well as its mean were determined (Table III). The selected perspective transform approximately halved the number of pixels. With respect to [1], the reduction was computed first and, therefore, information was lost during interpolation. Note that the Fourier spectrum of a discrete image is composed from a periodical repetition of the sampled spectrum corresponding to the continuous image. Decreasing the number of spatial data points also reduces the periodicity of this repeated spectra. It depends on the higher frequency characteristics whether the repeated spectra overlap. In other words, aliasing effects were introduced by inproper downsizing of images. As a result, the score tended to decrease for large FIR kernels [1, Table IV] and for higher degrees of B-spline interpolators (Table III). However, there was no statistical significance $(p > 0.005)$ within the large group of techniques resulting in scores $S_C \geq 0.82$.

Table IV shows the results of the modified third experiment. In order to fulfill the sampling theorem, the corresponding inverse perspective transform was applied resulting in a magnification of the intermediate image by approximately doubling the number of pixels. Although the standard deviation was about ten times larger than in the case of different transforms that were based on the same image (Table II), the improvement obtained by increasing stepwise the degree of B-spline interpolation was still statistically significant $(p \ll 0.005)$. Therefore, assuming no aliasing, the impact resulting from B-spline interpolation was independent of both the geometric transform as well as the specific content of an image.

D. Computational Complexity

Differences in complexity between the various interpolation and approximation methods directly result from the complexity of the kernel $h(x)$ and of the prefiltering step in case of B-spline interpolation. In general, a piecewise polynomial $h(x)$ of degree M requires M multiplications and M additions per sample point x. During the one-dimensional convolution, the polynomial $h_N(x)$ is evaluated at N sample points, resulting in $N \cdot M$ multiplications and additions. However, it depends on the specific polynomial whether all factors exist and, hence, the complexity at certain positions often is lower. For example in a straightforward implementation, the computation of the four cubic B-spline coefficients requires 12 multiplications and eight additions in total [1].

If B-spline interpolation is intended, the image must also be prefiltered. Unser *et al.* have developed a fast recursive algorithm, which in one dimension only needs $2\lfloor M/2 \rfloor$ additions and $2\lfloor M/2 \rfloor$ multiplications per sample point [8]. In the case of postfiltering with the cubic B-spline, these are two multiplications and two additions.

E. Runtime Measurements

The runtimes of the various interpolation schemes were measured on a Sun Ultra 1 (Fig. 7). A shell script was used to average 50 rotations of the MRI. Sources have been compiled using GNU's gcc version 2.95.2 without optimization, which

allows direct comparison with the runtimes of all other methods [1, Fig. 28].

The source code of the various B-spline interpolators was obtained in ANSI-C from the internet [9] and integrated without any modification. The internet distribution offers different degrees of splines, which were internally handled as variables, as well as two choices of boundary extrapolation. This resulted in some overhead, slowing down the computation. In comparison, the existing implementation of the cubic B-spline interpolator is specialized to the cubic degree only, but does not calculate the B-spline coefficients in a recursive manner. Since the quantitative error analysis was based on a centered subimage to ensure the results were independent of certain boundary handling, both B-spline implementations ran with the zero padding technique. This was fastest but offered only poor quality at the image margin.

The rotation of the 256×256 pixel coordinates took approximately 0.10 s. Simple methods such as nearest neighbor or linear interpolation were fastest and required less time for the interpolation itselve than for the rotation of the pixel coordinates. The interpolating B-splines of degrees ranging from $M = 2$ to $M = 5$ took between 0.57 and 1.01 s, which is between nine times to 18 times of the linear method, respectively. With efficient implementation, the runtimes of all B-splines are expected to reduce significantly. For example in the cubic case, a reduction from 0.59 to 0.26 s was measured (Fig. 7). This equals a speedup about more than 50%, only five times slower than the interpolation time for the linear method. Incorporating the recursive sheme for coefficient determination will further accelerate B-spline interpolation.

IV. Discussion

Image interpolation is as old as computer vision and several competitive techniques exist. As pointed out in [1], for any technique examples can be given where each scheme is advantageous. High-degree B-spline interpolation hold impressive spatial and Fourier properties as well as the lowest error in both, qualitative and quantitative analyses. Particularly for those applications in medical image processing that require supreme precision, high-degree B-splines are preferable interpolators.

Beside the runtime, there are some other aspects of B-spline interpolators the user should take care of. In contrast to the $1/x$-decay of the ideal sinc interpolation, the infinite B-spline interpolating kernels enjoy fast, exponential decay. Although the arbitrary extrapolation of data does not extend very far indeed, appropriate techniques for data extension over the known support of an image should be applied. Such techniques are described precisely in the literature and they are also available in C-code [9].

Furthermore, attention should be payed to the kind of geometric transform requiring the interpolation. In our third numerical investigation, the images are shrinked to approximately half the number of pixels before they are reconstructed again. Hence, a nonnegligible amount of aliasing takes place and interferes with interpolation. In particular, high image frequencies majorly are affected by aliasing during the downsampling step, which is independent of the interpolation or approximation technique in use. In our experiment, these distortions are preserved mainly by large-sized interpolators during the reconstruction step increasing the total error. Qualitatively spoken: the larger the spatial kernel size, the more sharp the interpolator's frequency response and the higher the maintained aliasing error that is observed in the third experiment (Table III). Although techniques exist that allow to predict exactly the amount of aliasing for each kernel [10], the satisfaction of Shannon's sampling theorem should always be guaranteed beside the proper choice of the interpolation method. In other words, appropriate smoothing of an image must be performed before reducing the number of pixels using any interpolation.

Acknowledgment

The authors would like to thank P. Thévenaz and M. Unser, Swiss Federal Institute of Technology, Lausanne, Switzerland, for their constructive comments on the manuscript.

References

[1] T. M. Lehmann, C. Gönner, and K. Spitzer, "Survey: Interpolation methods in medical image processing," *IEEE Trans. Med. Imag.*, vol. 18, pp. 1049–1075, Nov. 1999.

[2] M. Unser, "Splines—A perfect fit for signal and image processing," *IEEE Signal Processing Mag.*, vol. 16, pp. 22–38, June 1999.

[3] M. Unser, A. Aldroubi, and M. Eden, "B-spline signal processing: Part I—Theory," *IEEE Trans. Signal Processing*, vol. 41, pp. 821–833, Feb. 1993.

[4] ——, "B-spline signal processing: Part II—Efficient design and applications," *IEEE Trans. Signal Processing*, vol. 41, pp. 834–848, Feb. 1993.

[5] A. Aldroubi, M. Unser, and M. Eden, "Cardinal spline filters: Stability and convergence to the ideal sinc interpolator," *Signal Processing*, vol. 28, pp. 127–138, Feb. 1992.

[6] M. Unser, A. Aldroubi, and M. Eden, "Polynomial spline signal approximations: Filter design and asymptotic equivalence with shannon's sampling theorem," *IEEE Trans. Inform.. Technol.*, vol. 38, pp. 95–103, Jan. 1992.

[7] M. Unser, P. Thévenaz, and L. Yaroslavsky, "Convulotion-based interpolation for fast, high-quality rotation of images," *IEEE Trans. Image Processing*, vol. 4, pp. 1371–1381, Oct. 1995.

[8] M. Unser, A. Aldroubi, and M. Eden, "Fast B-splines transforms for continuous image representation and interpolation," *IEEE Trans. Pattern Anal. Machine Intell.*, vol. 13, pp. 277–285, Mar. 1991.

[9] P. Thévenaz. (2000, Mar.) Spline Interpolation [Online]. Available: http://bigwww.epfl.ch/thevenaz/interpolation

[10] T. Blu and M. Unser, "Quantitative Fourier analysis of approximation techniques: Part I—Interpolators and projectors," *IEEE Trans. Signal Processing*, vol. 47, pp. 2783–2795, Oct. 1999.